

WORD: A large scale dataset, benchmark and clinical applicable study for abdominal organ segmentation from CT image

Xiangde Luo^{1,4}, Wenjun Liao^{2,5}, Jianghong Xiao^{3,*}, Tao Song⁴, Xiaofan Zhang⁴, Kang Li⁶,
Dimitris N. Metaxas⁷, Guotai Wang^{1,*}, and Shaoting Zhang^{1,4,*}

¹School of Mechanical and Electrical Engineering, University of Electronic Science and Technology of China, Chengdu, China

²Department of Radiation Oncology, Sichuan Cancer Hospital and Institute, Sichuan Cancer Center

³Department of Radiation Oncology, Cancer Center West China Hospital, Sichuan University, China
⁴Shanghai AI Lab, Shanghai, China

⁵School of Medicine, University of Electronic Science and Technology of China, Chengdu, China

⁶West China Hospital-SenseTime Joint Lab, West China Biomedical Big Data Center, Sichuan University, Chengdu, China

⁷Department of Computer Science, Rutgers University, Piscataway, NJ 08854 USA

*Corresponding: xiaojh@scu.edu.cn, {guotai.wang, zhangshaoting}@uestc.edu.cn

Abstract

Whole abdominal organ segmentation plays an important role in diagnosing abdomen lesions, radiotherapy, and follow-up. However, oncologists' delineating all abdominal organ is time-consuming and very expensive. Recently, deep learning-based medical image segmentation has shown the potential to reduce manual delineation efforts, but it still requires a large-scale fine annotated dataset for training. Although many efforts in this task, there are still few large image datasets covering the whole abdomen region with accurate and detailed annotations for the whole abdominal organ segmentation. In this work, we establish a large-scale Whole abdominal ORgan Dataset (WORD) for algorithms research and clinical applications development. This dataset contains 150 abdominal CT volumes (30495 slices). Each volume has 16 organs with fine pixel-level annotations and scribble-based sparse annotation, which may be the largest dataset with whole abdominal organ annotation. Several state-of-the-art segmentation methods are evaluated on this dataset. And we also invited three clinical oncologists to revise the model predictions to measure the gap between the deep learning method and three oncologists. Afterward, we investigate the inference-efficiently learning on the WORD dataset, as the high-resolution image requires large GPU memory and inference time in the test stage. We further evaluate the scribble-based annotation-efficient

learning on this dataset, as the pixel-wise manual annotation is time-consuming and expensive. The work provided a new benchmark for the abdominal multi-organ segmentation task, and these experiments can serve as the baseline for future research and clinical application development. The codebase and dataset is released at: <https://github.com/Hilab-git/WORD>.

1. Introduction

Abdominal organ segmentation is a very fundamental and essential task in abdominal disease diagnosis, cancer treatment, and radiotherapy planning [41]. As accurately segmented organs can provide pieces of valuable information for the clinical diagnosis and follow-ups like organ size, location, boundary state, the spatial relationship of multiple organs, etc. In addition, organ segmentation plays an irreplaceable role in clinical treatment, especially in radiation therapy-based cancer and oncology treatments [8]. Accurate organs at risk segmentation can alleviate potential effects on healthy organs near cancer regions. However, organ segmentation is usually manually performed by radiation oncologists or radiologists in clinical practice. It is time-consuming and error-prone, as it requires annotators to delineate and check slice-by-slice and may take several hours per case. In addition, due to the different imaging pro-

Dataset	Year	Organ	Scans	NSD	AFS	WAR
BTCV [23]	2015	Spleen, Kidney (L), Kidney (R), Gallbladder, Esophagus, Liver, Stomach, Aorta, Inferior vena cava, Portal vein and splenic vein, Pancreas, Adrenal gland(L), Adrenal gland(R), Duodenum	50	✓	✓	✗
DenseVNet [14]	2018	Spleen, Kidney (R), Gallbladder, Esophagus, Liver, Stomach, Splenic vein, Pancreas and Duodenum	90	✗	✓	✗
CT-ORG [38]	2020	Lung, Bones, Liver, Kidneys and Bladder	140	✗	✗	✗
AbdomenCT-1K [32]	2021	Spleen, Kidney, Liver and Pancreas	1112	✗	✗	✗
WORD (ours)	2021	Liver, Spleen, Kidney(L), Kidney(R), Stomach, Gallbladder, Esophagus, Pancreas, Duodenum, Colon , Intestine , Adrenal(L), Adrenal(R), Rectum , Bladder, Head of Femur(L) and Head of Femur(R)	150	✓	✓	✓

Table 1. Summary of publicly available abdominal CT datasets. NSD: New Source Data; AFS: Annotate From Scratch. WAR: with the Whole Abdominal Region. To best our knowledge, there are very few datasets with **Colon**, **Intestine** and **Rectum** annotations.

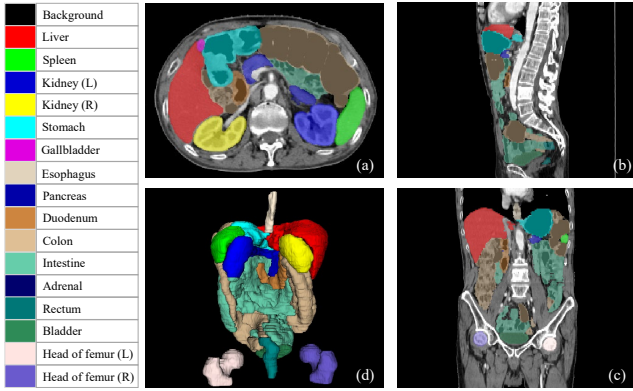


Figure 1. Scans in the WORD dataset are carefully annotated with 16 organs. The left table lists the annotated organs categories. (a), (b), (c) denote the visualization in axial, coronal, and sagittal views, respectively. (d) represents the 3D rendering results of annotated abdomen organs.

tocols/quality, and anatomical structures, fast delineation of a large number of organs is also a challenging task for junior oncologists [16].

Recently, many deep learning-based methods have been proposed to accurately and quickly segment organs from abdominal CT volumes [8, 32, 48]. However, these methods were evaluated on small or in-house datasets or just segmented very few organs. The main reason caused these problems is lacking an open available large-scale real clinical dataset with good whole abdominal organ annotation. AbdomenCT-1K [32] collected and annotated more than 1000 abdominal CT scans from existing datasets; each scan has four organs annotation. It further points out that abdominal organ segmentation is a solved problem for liver, spleen, kidney, and pancreas segmentation, but the whole abdominal organ segmentation remains an unsolved problem. BTCV [23] dataset has 50 CT volumes, and each volume has 13 organs annotations. DenseVNet [14] proposed a large dataset that includes 90 CT volumes with 8 organs annotation, where 47 volumes come from the BTCV [23] dataset and other 43 volumes from the TCIA [39] dataset

(NIH-Pancreas). Here, we review several widely-used datasets, some small datasets, just a few organs annotated datasets, or private or not available datasets, which have been out of the scope of this work.

Our goal is to collect a large-scale real clinical abdomen dataset with careful annotations. All scans in our dataset are manually segmented in great detail, covering all organs in the abdominal region. As we know that collecting such a dataset has many challenges. Due to privacy and ethical protection, collecting real clinical data is challenging and time-consuming. In addition, annotating a large-scale 3D medical image segmentation dataset is very expensive and time-consuming, as it requires domain knowledge and clinical experience. So many recent datasets used open datasets for further annotation or used the pre-trained model or semi-automatic methods to generate annotations and refinements. In contrast, our WORD was collected from a radiation therapy center and annotated by one senior oncologist (with seven years experience) and then checked by an expert of oncology (more than 20 years experience). Furthermore, the data consistency and quality are much higher than previous works. All of them were scanned before the radiotherapy treatment, without any appearance enhancement, with a similar scan location and with a similar image spacing, etc. Fig. 1 shows an example from our dataset.

Moreover, we investigate current methods on this dataset, including fully supervised segmentation methods and annotation-efficient methods. Specifically, we first evaluate several state-of-the-art medical segmentation methods on WORD data, like Convolutional Neural Network-based methods nnUNet [21], Attention UNet [35], DeepLabV3+ [7], UNet++ [58] and ResUNet [10] and Transformer-based CoTr [50] approaches and UNETR [18]. After that, we investigate the pre-trained model generalization ability on two open datasets. Due to previous datasets did not annotate too many organs, we further annotated an open dataset for generalization evaluation, where 20 cases with the whole abdominal region were selected and annotated manually from the LiTS [1] dataset. Afterwards, we do the user study on this dataset to measure the gap between

deep learning models and three oncologists. Considering these CT images have very high resolution, we investigate inference-efficient learning to reduce the memory and time costs and accelerate the inference procedure. Finally, we introduce a weakly supervised abdominal organ segmentation method with scribble annotations, which is desirable to reduce the annotation costs in the future. These attempts can be used as a new abdominal organ segmentation benchmark for further research.

In summary, our contribution is two-fold:

- 1) We build a large-scale whole abdominal organ segmentation dataset that is a real clinical dataset and has more categories and higher quality annotations. In addition, we further annotate 20 cases from LiTS [1] for networks' generalization evaluation.
- 2) We establish a new abdominal organ segmentation benchmark by (1) evaluating the existing segmentation methods, (2) measuring the gap between deep learning models and oncologists, (3) investigating the pre-trained model generalization ability on open datasets, (4) investigating the inference-efficient learning for the high-resolution abdominal CT image segmentation, (5) introducing scribble-based weakly supervised methods to reduce the label costs.

2. Related work

2.1. abdominal organ segmentation datasets

Since clinical CT images with the whole abdominal region are very private and challenging to collect and annotate, few openly available datasets are available. We summarize these publicly available abdominal CT datasets in Tab. 1. We consider the dataset, which has four or more annotated organs in this work. The BTCV (Beyond The Cranial Vault) [23] consists of 50 CT volumes, where 30 and 20 volumes are used for training and testing, respectively. In the BTCV dataset, 13 organs are annotated manually, including the aorta, liver, spleen, right kidney, left kidney, stomach, pancreas, gallbladder, esophagus, inferior vena cava, portal vein and splenic vein, right adrenal gland, and left adrenal gland. The DenseVNet [14] has 90 CT scans, where 47 scans come from the BTCV dataset [23], and the other 43 cases come from TCIA data [39] each of them has eight organs annotation. The CT-ORG [38] is an open dataset that contains 140 CT images, and five organs are annotated. Most of these images come from a challenge training set [1]. The AbdomenCT-1K dataset [32] extended five open single-class organs annotation datasets to four classes (with 1062 volumes) and a small clinical dataset (with 50 volumes coming from 20 patients). This dataset contains four organ annotations: liver, kidney, spleen, and pancreas. BTCV, DenseNet, and CT-ORG are limited by the small

scale or few annotated classes to boost this topic research. Although AbdomenCT-1K is huge, the annotated organs are also too few to evaluate the efficiency of the whole abdominal segmentation task. Unlike these existing datasets, our dataset comes from a new medical center with a large scale and more annotated organs, such as colon, intestine, rectum, etc. We believe that this dataset is one of the most comprehensive ones in medical image segmentation datasets.

2.2. abdominal organ segmentation methods

Recently, deep learning-based methods have been widely used in abdominal organ segmentation tasks, especially the UNet-based deep networks. The main challenge in this task lies in complex anatomical structures, the unclear boundary of soft tissues, high resolution of images, and extremely unbalanced sizes among large and small organs, etc. Many works have also been attempted to handle these challenges. [14] proposed a dense V-network to segment 8 organs from CT volumes, which enables high-resolution activation maps through memory-efficient dropout and feature reuse. [48] presented a novel framework for abdominal multi-organ segmentation by using organ-attention networks with reverse connections and evaluated it on an in-house dataset. [25] combined the inter-and intra-patient deformation data augmentation with multi-scale Attention-UNet [40] for accurate abdominal multi-organ segmentation. [44] proposed a batch-based method plus random shifting strategy to boost the performance of multi-organ segmentation from high-resolution abdomen CT volumes. More recently, transformer-based methods [2, 5] is used to explicitly model the long-range dependence to capture the relationship of multi-organ for accurate segmentation. Although the above methods have achieved promising results, they are also limited by requiring large scale carefully annotated dataset. To reduce label costs, [57] proposed a co-training-based semi-supervised method for abdominal multi-organ segmentation, which reduces almost half of annotation costs. Furthermore, [56] proposed a prior-aware neural network that incorporates anatomical priors on abdominal organ sizes to train models from several partially-labeled datasets. This work first investigates more annotation-efficient abdominal multi-organ segmentation methods with very sparse annotations (scribbles). In addition, we investigate inference-efficient learning for the segmentation of high-resolution abdominal CT images to reduce the memory and time costs in the test stage.

3. WORD: Fully Annotated Clinical Whole abdominal organ Dataset

3.1. Dataset summary

The 150 CT scans in the WORD were collected from 150 patients before the radiation therapy, and these patients

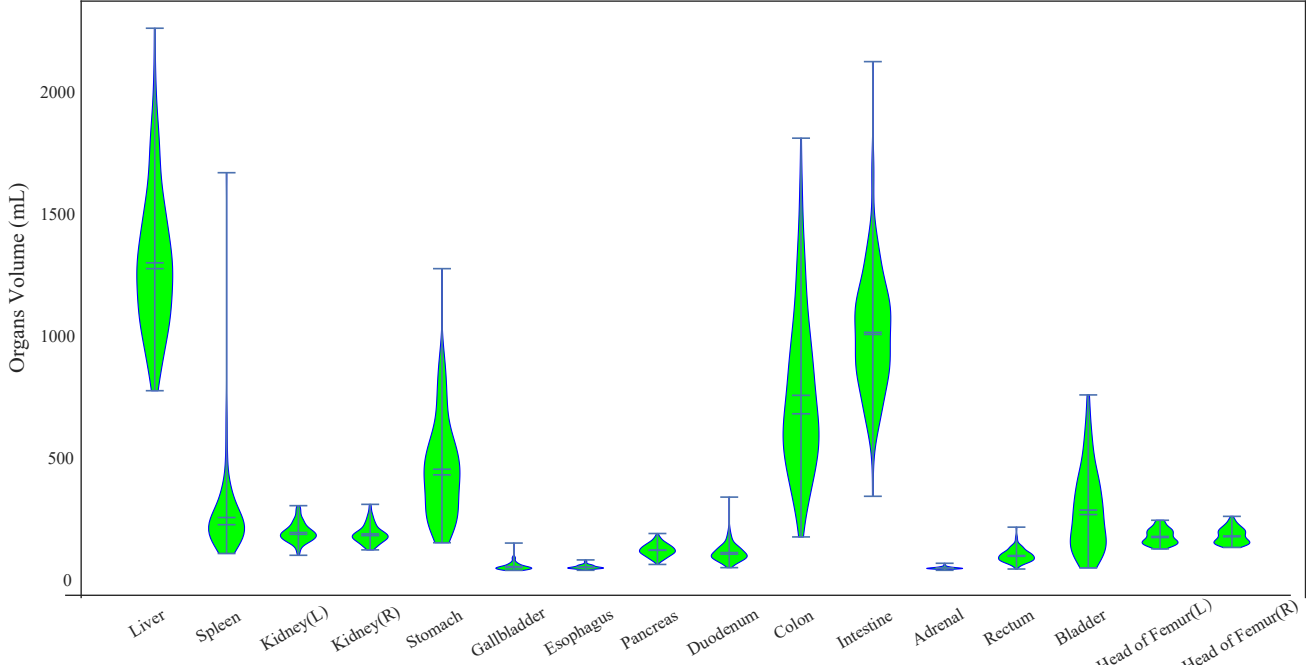


Figure 2. Volume distribution of each organ in the WORD.

were suffered from prostatic cancer, cervical cancer, or rectal cancer. Each CT volume consists of [159 - 330] slices of 512×512 pixels, with an in-plane resolution of $0.976 \text{ mm} \times 0.976 \text{ mm}$ and slice spacing of $2.5\text{-}3.0 \text{ mm}$, indicating that the WORD is a very high-resolution dataset. All scans of WORD are exhaustively annotated with 16 anatomical organs, including the liver, spleen, kidney (L), kidney (R), stomach, gallbladder, esophagus, duodenum, colon, intestine, adrenal, rectum, bladder, head of the femur (L) and head of the femur (R). An example of image and annotation from the WORD dataset is shown in Fig. 1. All images were anonymized and approved by the ethics committee to protect privacy where all clinical treatment details have been deleted. We randomly split WORD into three parts: 100 scans (20115 slices) for training, 20 scans (4103 slices) for validation, and 30 scans (6277 slices) for testing. Fig. 2 shows the volume distributions of all annotated organs. It shows that the very extreme unbalanced distribution among large and small organs, which may bring some challenges to this task. At the same time, We further selected and annotated 20 CT scans from LiTS [1] as a generalization and external evaluation set. Similar to WORD, these scans cover the whole abdominal region, and each scan has 16 organ annotations. In the future, the total number of images and annotated organs in the WORD will still be updated.

3.2. Professional data annotation

Recently, the AbdomenCT-1K dataset [32] established an abdominal organ dataset by using the pre-trained model

for predictions and then refining by radiologists. At the same time, CT-ORG [38] annotated abdominal organ by using a semi-automatic tool firstly (ITK-SNAP [52]) and then refining manually. However, these initial segmentation results could affect the annotator’s decision, especially in boundary regions with low contrast. Different from AbdomenCT-1K [32] and CT-ORG [38], all scans in the WORD dataset are annotated from scratch manually. A senior oncologist (with seven years of experience) uses ITK-SNAP [52] to delineate organs slice-by-slice in axial view. After that, an expert in oncology (more than 20 years of experience) checks these annotations carefully. Note that all annotations obey the radiation therapy delineation guideline published by Radiation Therapy Oncology Group (RTOG)¹. In the annotation stage, each volume roughly takes 1.2-2.6 hours to annotate all 16 organs and further requires 0.4-1.0 hours to check and refine the annotation. The WORD dataset takes us around 15 months to collect, annotate and review, so we think it’s precious and desirable to share with the medical image analysis community.

3.3. Potential research topics

We can conduct many essential research topics on medical image segmentation/detection methods and clinical applications with the large and carefully annotated abdominal multi-organ dataset. Besides, there are some challenges in the WORD dataset, including the imbalanced sample

¹<https://www.rtog.org/>

Method	Liver	Spleen	Kidney(L)	Kidney(R)	Stomach	Gallbladder	Esophagus	Pancreas	Duodenum	Colon	Intestine	Adrenal	Rectum	Bladder	Head of Femur(L)	Head of Femur(R)	Mean
nnUNet(2D)	95.38±4.45	93.33±11.85	90.05±19.35	89.86±19.56	78.43±16.48	78.08±13.99	82.33±6.5	63.47±15.81	83.06±8.32	85.6±4.08	69.9±11.07	81.66±6.64	90.49±14.73	93.28±5.31	93.78±4.38	84.92±5.39	
nnUNetV2(2D)	96.19±2.46	94.33±2.74	91.29±18.15	91.20±17.22	91.12±3.60	89.19±12.15	77.79±13.51	83.55±5.87	64.67±15.87	83.92±8.45	86.83±4.02	70.0±11.86	90.15±6.73	93.28±5.12	93.93±4.29	85.80±5.37	
ResUNet(2D)	96.53±0.89	95.26±2.84	95.63±1.20	95.84±1.16	91.58±2.86	82.83±11.8	77.17±14.68	83.56±5.60	66.67±15.26	83.57±8.69	86.76±3.56	70.9±10.12	82.16±6.73	91.0±13.5	93.39±5.11	93.88±4.30	86.67±4.81
DeepLabV3+(2D)	96.21±1.34	94.68±5.64	92.01±13.00	91.84±14.41	91.16±3.07	80.05±17.92	74.88±14.69	82.39±6.68	62.81±15.21	82.72±8.79	85.96±4.02	66.82±10.81	81.85±6.67	90.86±14.07	92.01±4.76	92.29±4.01	84.91±5.05
UNet++(2D)	96.33±1.40	94.64±4.22	93.36±5.06	93.34±7.38	91.33±3.13	81.21±12.24	78.36±12.84	84.43±6.77	65.99±15.79	83.22±8.98	86.37±4.01	71.04±10.65	81.44±6.7	92.09±11.53	93.38±5.12	93.88±4.21	86.28±3.96
AttUNet(3D)	96.00±1.01	94.90±1.63	94.65±1.38	94.7±2.78	91.15±2.74	81.38±12.24	76.87±15.12	83.55±6.2	67.68±14.01	85.72±8.50	88.19±3.34	70.23±9.31	80.47±5.44	91.90±4.39	92.43±3.68	86.21±4.78	
nnUNet(3D)	96.45±0.85	95.98±0.89	95.40±0.95	95.68±1.07	91.69±2.5	83.19±8.81	78.51±12.22	85.04±5.78	68.31±16.29	87.41±7.38	89.3±2.75	72.38±8.98	82.41±4.9	92.59±8.27	91.99±4.72	92.74±3.63	87.44±4.33
nnUNetV2(3D)	96.59±6.6	96.09±8.10	95.63±9.20	95.83±9.00	91.57±3.05	83.72±8.19	77.36±13.68	85.00±5.95	67.73±16.75	87.26±8.25	89.37±3.11	72.98±8.09	82.32±5.26	92.11±9.75	92.56±4.19	92.49±4.03	87.41±4.57
UNETR(3D)	94.67±1.92	92.85±3.03	91.49±5.81	91.72±6.12	65.08±19.63	67.71±13.46	74.79±9.31	57.56±11.53	74.62±11.5	80.4±8.32	74.06±8.03	85.42±8.17	89.47±6.64	90.17±4.40	79.77±4.92		
CoTr(3D)	95.58±1.59	94.99±1.37	93.26±3.07	93.63±3.00	89.99±4.49	76.4±16.49	74.37±14.92	81.02±7.23	63.58±14.88	84.14±7.82	86.39±3.51	69.06±9.26	80.0±5.43	89.27±18.28	91.03±4.81	91.87±3.32	84.66±5.45

Table 2. Comparison between various SOTA segmentation methods in term of *DSC*(%)

Method	Liver	Spleen	Kidney(L)	Kidney(R)	Stomach	Gallbladder	Esophagus	Pancreas	Duodenum	Colon	Intestine	Adrenal	Rectum	Bladder	Head of Femur(L)	Head of Femur(R)	Mean
nnUNet(2D)	7.94±17.23	14.46±41.27	10.53±29.43	10.73±28.49	19.04±20.82	8.9±10.33	6.6±9.72	7.92±7.34	25.18±18.39	15.56±12.97	10.46±6.24	6.06±3.99	10.62±5.5	5.88±8.09	5.89±7.55	10.79±10.29	
nnUNetV2(2D)	7.34±16.48	9.53±33.84	10.33±29.52	10.85±28.41	13.97±12.08	7.91±8.67	6.7±7.8	7.82±6.76	23.29±14.39	15.68±14.0	8.96±4.83	6.42±4.3	11.15±7.33	4.97±5.26	5.54±8.13	9.88±9.16	
ResUNet(2D)	4.64±7.37	8.7±30.11	5.4±15.85	2.47±0.97	9.98±6.62	4.6±7.6	6.7±7.6	7.82±7.83	21.79±12.83	17.41±15.22	6.67±4.59	10.62±6.52	5.02±6.17	6.56±8.3	5.98±7.2	8.6±6.47	
DeepLabV3+(2D)	6.81±18.3	8.93±33.61	10.49±29.39	10.02±28.08	11.01±8.45	7.36±9.43	7.6±8.45	7.67±7.1	21.61±13.88	15.95±14.07	5.97±5.21	7.14±4.8	10.96±6.93	5.14±6.22	7.62±7.93	7.02±6.76	9.67±9.06
UNet++(2D)	11.77±22.17	9.39±32.14	13.09±29.75	21.84±42.61	15.4±21.44	14.68±28.48	5.85±3.93	7.5±4.45	23.67±13.36	16.97±13.92	10.06±6.01	11.44±4.97	11.54±8.13	5.06±6.56	6.66±8.22	16.92±6.03	12.35±15.75
AttUNet(3D)	3.61±1.75	2.74±1.61	6.28±19.19	2.86±4.66	8.24±3.06	5.11±3.41	5.35±3.79	6.96±7.39	21.61±12.86	20.12±12.87	5.68±3.93	11.67±6.37	4.83±4.66	6.93±6.27	6.06±7.78	7.13±4.68	
nnUNet(3D)	3.31±1.38	2.15±0.5	6.07±19.38	2.35±3.03	8.47±3.59	5.24±3.3	5.49±4.2	6.84±7.39	21.31±14.22	19.99±13.17	5.14±4.83	5.46±4.04	11.57±6.95	3.68±2.23	35.18±88.78	33.09±32.19	10.33±10.65
nnUNetV2(3D)	3.17±0.51	2.12±0.47	2.46±0.7	2.24±0.47	9.47±7.61	6.04±6.53	5.83±4.64	6.87±7.86	21.15±14.26	10.42±14.27	5.27±4.29	5.43±3.82	12.39±8.12	4.17±3.6	17.05±62.15	27.29±9.62	8.84±22.63
UNETR(3D)	8.36±14.13	14.84±34.62	23.37±39.28	7.9±19.08	19.25±23.19	12.72±15.59	9.31±8.41	8.66±8.56	25.15±21.96	20.32±14.37	12.62±7.63	8.73±5.3	12.79±6.38	4.77±1.82	38.11±98.44	38.62±99.75	17.34±23.88
CoTr(3D)	7.47±12.37	8.14±24.43	16.42±27.79	12.79±29.76	10.26±9.49	11.32±15.57	6.29±4.53	8.88±10.61	24.85±15.47	12.41±12.75	7.96±5.58	6.76±6.99	14.34±35.85	19.42±70.83	26.78±74.8	12.83±21.96	

Table 3. Comparison between various SOTA segmentation methods in term of *HD*₉₅(mm)

among large and small size organs, the high resolution, the complex anatomical structure. It can be used to develop or evaluate clinical applications, as it is very desirable to develop a tool or software to assist oncologists in delineating organs quickly and accurately. The WORD dataset also can be employed in general algorithms research, such as fully-/semi-/weakly-supervised learning, domain adaption/generalization, partially label and lifelong learning, etc. Here, we roughly summarized the potential research topics as follows:

Fully-supervised abdominal organ segmentation: (1) Fully supervised learning [21] aims to efficiently utilize the labeled data to achieve good results and solve the imbalanced distributions and complex structures challenges. It is a fundamental topic and has been studied for many years. Here, we presented a new dataset, WORD, to boost abdominal organ segmentation algorithm research, evaluation, and comparison. In addition, the WORD also can be used to develop clinical applications or clinically applicable evaluations.

Abdominal organ segmentation with low computational costs and high speed: For 3D abdominal CT scans, due to the high dimension and resolution, the inference stage always takes much time and GPU memory. To deal with this issue, inference-efficient learning [13] is proposed to achieve the trade off between high performance and low inference costs. However, there are very few works that have been studied to accelerate the inference of 3D medical image segmentation tasks [44]. Recently, knowledge distillation has achieved success in several 2D natural image tasks inspiring us that knowledge distillation may have the potential to handle the 3D medical image segmentation tasks [33].

Abdominal organ segmentation with low annotation cost: Pixel-wise abdominal organ annotation is very expensive, as it requires clinical experience and much time. Recently, annotation-efficient learning [28, 57, 29] has been introduced to reduce the label costs and improve the network generalization ability by semi-/weakly-supervised learning,

domain adaptation strategies, etc. These strategies have been scorching topics and show the potential to reduce annotation costs by utilizing unlabeled data or sparse annotations. It is desirable to reduce the annotation cost for accurate abdominal organ segmentation, as it can accelerate the model development and reduce the costs. In this work, we pay more attention to evaluating weakly supervised methods to reduce the label costs.

4. Experiments and Analyses

4.1. Implementations and metrics

In this work, all methods are implemented, trained, and tested by PyTorch 1.8 [36] on a cluster with eight NVIDIA GTX1080TI GPUs. We chose the powerful nnUNet² [21] as our baseline for fair comparisons. As it is a self-configuration segmentation framework without needing any manual effort for data processing, training planning (network architectures and parameters setting, etc.), and post-processing, and has won more than 19 medical segmentation challenges [21]. Due to the nnUNet just providing the vanilla UNet network, we further adapt it to support more network architectures. Note that we use the public implementations of the compared methods³. We employ the default settings of nnUNet as our experimental settings, where the batch size is 2 for 3D methods and 12 for 2D methods, the total epoch is 1000, and the loss function is a combination of cross-entropy and dice loss. All the models are trained and tested based on the default settings, except we don't use the test time augmentation. And each model needs more than six GPU days to train, and each volume takes more than five minutes to infer. We use two widely-used metrics to measure the segmentation quality in this work. Dice similarity coefficient (*DSC*) is used to evaluate the pixel-wise overlap between the ground truth and prediction. In addition, we also measure the 95% Hausdorff Distance (*HD*₉₅) between the boundaries of the ground truth and

²<https://github.com/MIC-DKFZ/nnUNet>

³https://github.com/qubvel/segmentation_models. pytorch

prediction. The implementations of DSC and HD_{95} are available⁴.

4.2. Fully-supervised abdominal organ segmentation

We first evaluate some existing state-of-the-art (SOTA) methods on the WORD. Then, we further evaluate the gap between the deep network and three oncologists. Finally, we investigate the domain shift between the WORD and three public datasets (BTCV [23] and TCIA [39], LiTS [1]).

4.2.1 Evaluations of SOTA methods on the WORD

For deep learning-based clinical applications, fully supervised learning is one of the most basic and popular solutions, especially in automatic multi-organ delineation systems. In this work, we investigate several existing SOTA methods on the WORD, including convolutional neural networks-based networks, nnUNet [21] and its variations (both 2D and 3D), ResUNet [10], DeepLabV3+ [7], UNet++ [58] and Attention-UNet (AttUNet) [35] and transformer-based architectures, CoTr [50] and UNETR [18]. The quantitative segmentation results in term of DSC and HD_{95} are presented in Tab. 2 and Tab. 3. It can be found that all SOTA methods can achieve very promising results on large organs, such as the liver, spleen, kidney, stomach, bladder, and head of the femur. At the same time, it also shows that all CNN-based methods outperform transformer-based CoTr [50] and UNETR [18]. It has also proven that the large organs segmentation task is a well-solved problem if there are enough high-quality annotated samples. But for small organs, it remains very challenging and also desires to pay more attention, especially for some extremely small and unclear boundary organs adrenal and duodenum. However, there are very few works and researchers that focus on these challenging tasks. One of the key reasons lies in lacking large-scale and public available datasets. To solve this dilemma, we build the baseline and dataset to boost further research in the medical computing community.

4.2.2 User study by three oncologists

Then, we employ a comprehensive user study to measure the gap between the network and three oncologists. Following the general workflow of deep learning-assisted organs delineation systems [8], we invite three junior oncologists (with 1-3 years of experience) from three different hospitals to revise model-generated predictions independently until the results are clinically acceptable. We randomly selected 20 predictions produced by nnUNetV2 (3D) for the

user study and calculated the revised results. The quantitative comparison in terms of DSC between the nnUNet predictions and three oncologists' revised results is presented in Fig. 3. For large size and clear boundary organs, the deep network can produce promising results that are very close to clinically applicable just with a few revisions. However, there is a massive gap between the deep network and junior oncologists in small organs segmentation. It indicates that the deep network has the potential to reduce the burden of oncologists in the large size of organs delineation. In the future, combining the user interaction with the deep network may help further to reduce the small size of organs delineation burden and accelerate the clinical workflow [31, 47].

4.2.3 Generalization on BTCV [23], TCIA [39] and LiTS [1]

We further investigate the domain shift between the WORD dataset and three widely-used public datasets BTCV [23], TCIA [39] and LiTS [1]. The differences between the WORD and BTCV [23], TCIA [39] and LiTS [1] lie in 1) coming from different centres/scanners/countries; 2) suffering from different diseases; 3) with different phase/contrast enhancement; 4) with different voxel spacing; 5) annotating by different oncologists/radiologists. All of them could affect the generalizability of the deep network and further limit clinical practice. In this work, we use the pre-trained model on the WORD dataset to infer the samples from BTCV [23] (47 scans), TCIA [39] (43 scans) and LiTS [1] (20 scans) to estimate the domain gap. Tab. 4 and Tab. 5 list the results of DSC and HD_{95} . Here, we just consider the official annotated organs of the BTCV [23] and TCIA [39] datasets. It can be found that there are very significant domain shifts between WORD and BTCV [23], TCIA [39] datasets, as the pre-trained nnUNet on the WORD dataset performs very worse on the BTCV [23] and TCIA [39]. For the LiTS [1] dataset, the nnUNetV2(3D) achieves very encouraging results, even better than the results of WORD. But the nnUNetV2(2D) still performs very bad; maybe the 3D spatial information can boost the network's generalization. It also indicates that the model generalization for the multi-site abdominal organ task is not a solved problem. Figure 4 shows some segmentation results of different datasets. These results are generated by a pre-trained nnUNetV2(3D) on the WORD dataset. It can be observed that the results of TCIA and BTCV are inaccurate, which indicates that there is a significant domain gap between TCIA/BTCV and WORD. In contrast, the result of LiTS is better and more promising; the reason may be the domain gap between LiTS and WORD is minor.

⁴<https://github.com/loli/medpy>

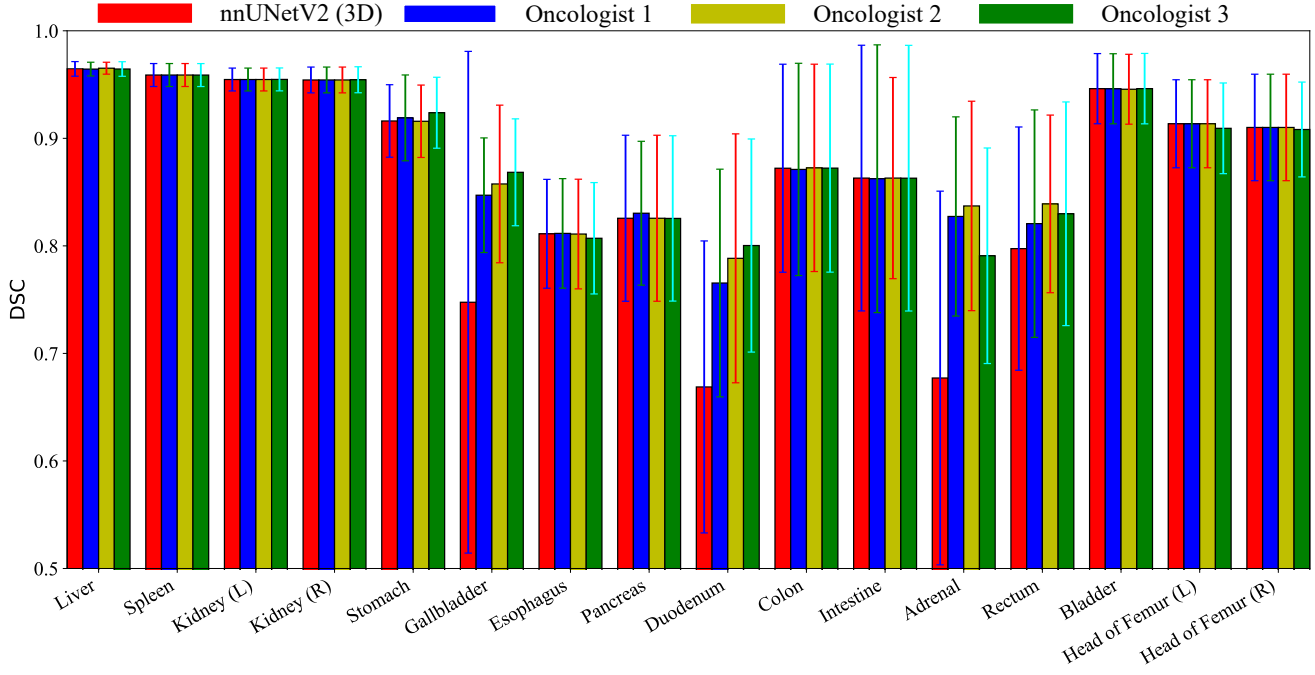


Figure 3. User study based on three junior oncologists independently, each of them comes from a different hospital.

DataSet	Method	Liver	Spleen	Kidney(L)	Kidney(R)	Stomach	Gallbladder	Esophagus	Pancreas	Duodenum	Colon	Intestine	Adrenal	Rectum	Bladder	Head of Femur(L)	Head of Femur(R)	Mean
TCIA	nnUNetV2 (2D)	91.27±3.71	85.47±13.97	80.34±13.4	-	54.32±21.73	54.0±32.36	54.62±21.38	51.38±15.59	33.15±18.92	-	-	-	-	-	-	63.06±7.79	
	nnUNetV2 (3D)	92.59±3.72	86.31±12.57	91.44±5.13	-	73.37±17.35	78.49±18.33	61.22±18.85	68.53±15.25	51.14±15.78	-	-	-	-	-	-	75.39±5.50	
BTCV	nnUNetV2 (2D)	86.63±7.79	72.43±19.36	64.57±23.94	37.32±33.71	51.73±22.74	40.38±32.44	49.64±17.59	24.19±14.78	-	-	-	-	-	-	-	49.10±7.34	
	nnUNetV2 (3D)	93.36±5.75	88.89±11.78	87.36±16.25	56.22±42.99	78.52±18.54	63.82±32.05	62.53±15.28	73.64±13.15	56.19±15.62	-	-	-	-	-	-	70.23±10.97	
LiTS	nnUNetV2 (2D)	92.37±3.48	84.73±14.43	79.23±22.39	78.51±22.39	68.46±15.88	49.05±32.97	48.77±5.04	59.59±12.78	45.01±15.52	75.42±14.65	64.35±10.77	62.86±14.16	68.93±24.83	91.63±5.94	93.26±2.37	92.73±3.12	74.43±8.29
	nnUNetV2 (3D)	94.2±1.41	95.28±5.44	96.33±3.83	96.07±4.84	86.43±13.68	60.15±34.37	87.13±6.8	89.43±4.16	76.45±6.4	87.54±8.32	83.6±6.87	85.89±4.49	80.61±19.57	92.88±7.43	95.55±2.63	94.98±3.51	87.66±7.98

Table 4. The DSC results on BTCV [23], TCIA [39] and LiTS [1] datasets using the pre-trained model on the WORD dataset.

4.3. Abdominal organ segmentation with low computational costs and high speed

Although large-scale deep models have achieved promising results for abdominal organ segmentation [21, 56, 44], these heavy models require various expensive computations and storage components and a long inference time [37]. In addition, the whole abdominal CT image has a very high resolution, which further increases the GPU memory budget and computational cost [37, 44]. So, it is desirable to investigate the high-performance and low computational costs method for abdominal organ segmentation, and it is also suitable for clinical scenarios. This study investigates the efficient abdominal organ segmentation topic and compares several lightweight network-based and knowledge distillation methods on the WORD dataset. Firstly, we compare three lightweight segmentation networks' performance in abdominal organ segmentation, ESPNet [34], DMFNet [4] and LCOVNet [55]. ESPNet [34] proposed an efficient spatial pyramid block for high-speed brain tumour segmentation. DMFNet [4] combined point-wise [54], group-wise [9] and atrous [6] convolutions to reduce the computational cost and boost brain tumour segmentation performance. LCOVNet [55] proposed a attention based spatio temporal separable convolution for efficient COVID-

19 pneumonia lesion segmentation. Afterwards, we study the knowledge distillation strategy for the efficient high-resolution image segmentation [20]. In general, knowledge distillation aims to transfer the knowledge of a heavy model (teacher) to a lightweight model (student) and encourages the student to achieve similar or comparable results to the teacher. Following the general knowledge distillation [20, 37], we used a pre-trained nnUNetV2(3D) as the teacher model and employed the logit output of nnUNetV2(3D) to guide the student models (ESPNet, DMFNet and LCOVNet). Table 6 and 7 list the quantitative results of different methods in terms of DSC and HD_{95} . It can be observed that the knowledge distillation strategy can improve student models' performance. In Table 8, we further analyze the model complexity of the teacher network and student networks in the same software and hardware environments ⁵. These results show that combining lightweight networks and knowledge distillation can achieve a trade-off between performance and computational costs. This study further indicates that exploring more power lightweight networks and knowledge distillation strategies is a potential solution for high performance, fast-speed and low computational cost abdominal organ segmentation [13, 37].

⁵<https://github.com/sovrasov/flops-counter.pytorch>

DataSet	Method	Liver	Spleen	Kidney(L)	Kidney(R)	Stomach	Gallbladder	Esophagus	Pancreas	Duodenum	Colon	Intestine	Adrenal	Rectum	Bladder	Head of Femur(L)	Head of Femur(R)	Mean
TCIA	nnUNetV2 (2D)	29.39±20.67	87.32±69.61	92.93±49.56	-	43.17±23.49	34.94±40.91	17.41±9.98	31.37±8.59	34.09±14.13	-	-	-	-	-	-	46.33±20.34	
	nnUNetV2 (3D)	17.11±24.27	31.28±59.62	15.43±39.47	-	26.75±22.9	7.65±11.62	15.85±9.66	15.59±13.67	35.07±18.54	-	-	-	-	-	-	20.57±12.30	
BTCV	nnUNetV2 (2D)	44.73±36.15	128.28±59.62	107.0±40.9	71.58±43.5	65.47±42.91	53.34±61.11	22.55±15.17	30.15±15.12	50.97±28.19	-	-	26.28±37.47	-	-	-	60.00±15.01	
	nnUNetV2 (3D)	13.96±23.73	37.46±67.09	20.34±38.08	27.8±28.6	31.42±40.64	16.69±21.8	18.81±18.02	13.12±18.01	29.0±15.09	-	-	5.20±9.75	-	-	-	21.39±15.96	
LiTS	nnUNetV2 (2D)	32.28±27.58	90.59±63.72	96.44±51.64	69.78±64.44	47.33±31.66	28.22±38.44	4.44±2.17	27.21±11.79	25.97±9.99	31.89±14.66	31.15±10.63	6.10±3.27	44.38±111.99	33.46±117.57	32.35±115.82	59.42±161.8	41.31±47.99
	nnUNetV2 (3D)	11.57±9.76	12.13±21.25	10.16±34.59	17.87±28.48	18.63±22.57	5.94±8.08	4.93±3.66	15.75±9.52	24.82±45.11	12.11±6.55	2.22±0.72	10.27±9.8	54.35±149.16	30.88±116.82	58.08±162.04	18.86±50.87	

Table 5. The HD_{95} results on BTCV [23], TCIA [39] and LiTS [1] datasets using the pre-trained model on the WORD dataset.

Method	Liver	Spleen	Kidney(L)	Kidney(R)	Stomach	Gallbladder	Esophagus	Pancreas	Duodenum	Colon	Intestine	Adrenal	Rectum	Bladder	Head of Femur(L)	Head of Femur(R)	Mean
Teacher (nnUNetV2(3D))	96.59±6.10	96.09±8.10	95.63±9.20	95.83±9.00	91.57±3.05	83.72±8.19	77.36±13.66	85.00±5.95	67.73±16.75	87.26±8.25	89.37±3.11	72.98±8.09	82.32±5.26	92.56±4.19	92.49±4.03	87.41±4.57	
ESPNNet	76.47±19.12	84.54±19.81	85.23±20.96	89.05±15.74	82.87±12.06	49.02±29.45	59.46±23.21	56.35±21.93	38.39±22.04	71.54±12.12	72.44±8.26	35.41±20.05	72.48±9.46	89.83±8.59	84.32±4.98	70.45±7.29	
ESPNNet-KD	94.10±1.92	94.01±1.03	91.81±1.81	91.72±1.06	65.08±0.93	55.56±1.21	71.71±1.46	77.70±1.23	72.56±1.15	60.76±0.32	74.08±0.83	85.42±0.17	90.17±0.17	97.77±0.22	-	-	
DMFNet	95.81±0.79	94.25±2.15	94.72±0.97	95.03±1.12	89.69±3.45	71.12±1.75	74.41±12.08	81.9±6.58	63.96±16.44	83.77±8.45	86.38±3.77	68.26±7.83	79.24±7.09	87.54±17.11	91.71±4.44	92.04±3.22	84.74±5.65
DMFNet+KD	95.96±0.76	94.64±2.53	94.71±1.01	94.96±1.19	89.88±5.24	79.84±1.81	74.1±14.81	81.66±7.12	66.66±16.18	83.51±7.68	86.05±3.11	66.73±8.13	79.26±8.57	88.18±15.91	91.99±4.61	92.55±3.93	85.1±5.09
LCOVNet	95.37±1.2	94.6±2.08	94.78±1.18	95.08±1.14	90.06±3.32	75.48±13.46	76.51±11.87	81.46±9.11	66.55±16.02	85.61±7.19	87.36±3.55	70.08±8.67	80.64±7.21	87.6±15.88	91.74±4.36	92.0±3.58	85.31±5.02
LCOVNet+KD	95.89±0.58	95.4±2.14	95.17±1.13	95.78±0.84	90.86±3.82	78.87±11.8	74.55±13.55	82.59±7.54	68.23±15.04	84.22±7.32	87.19±3.06	69.82±8.54	79.99±6.82	88.18±17.64	92.48±3.75	93.23±3.46	85.82±4.89

Table 6. Comparison between various efficient segmentation methods in term of $DSC(\%)$

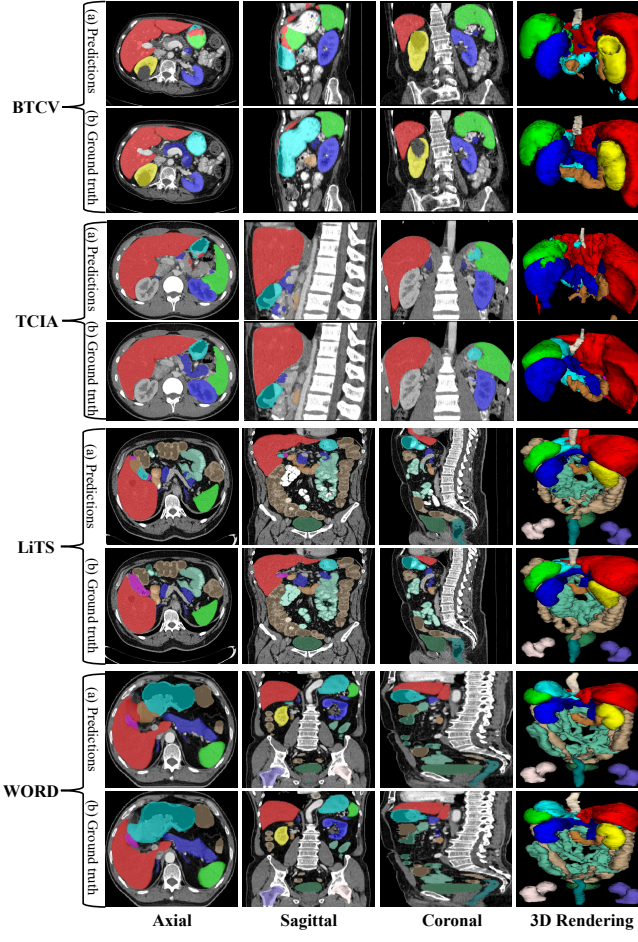


Figure 4. Visualizations comparison of different datasets. All predictions are produced by a pre-trained nnUNetV2 (3D) on the WORD dataset.

4.4. Abdominal organ segmentation with low annotation cost

Recently, many annotation efficient learning-based works have been employed to reduce medical image annotation costs [24, 28, 30, 49]. However, most of them are semi-supervised learning-based methods, which still need to annotate part of the dataset carefully. Weakly supervised

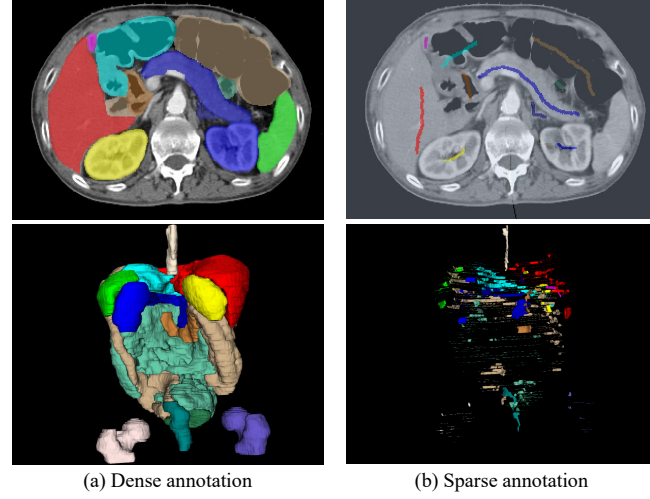


Figure 5. Different types of medical image annotation, the first and second rows show the visualization in 2D and 3D spaces, respectively.

learning just requires very few sparse annotations to learn and achieve promising results [26, 45]. Fig. 5 shows an example of different types of medical image annotation. It shows that the sparse annotation just requires very few label costs, less than 4% compared with dense annotation. In this work, we evaluate several weakly-supervised methods on the abdominal multi-organ segmentation task for the first time and further propose a new method to boost the results.

4.4.1 Learning from scribbles

To learn from scribble annotations, the general method is using the partially Cross-Entropy (pCE) loss to train deep networks, where just labelled pixels are considered to calculate the gradient and the other pixels are ignored [42]. However, due to the extremely sparse supervision, the pCE loss can not achieve promising results. To solve this dilemma, Tang et al. [43] proposed to integrate the pCE loss and MRF/CRF regularization terms to train deep networks with scribble annotations. After that, most of the recent weakly-supervised methods trained deep networks by using the fol-

Method	Liver	Spleen	Kidney(L)	Kidney(R)	Stomach	Gallbladder	Esophagus	Pancreas	Duodenum	Colon	Intestine	Adrenal	Rectum	Bladder	Head of Femur(L)	Head of Femur(R)	Mean
Teacher	3.17 \pm 0.51	2.12 \pm 0.47	2.46 \pm 0.7	2.24 \pm 0.47	9.47 \pm 7.61	6.04 \pm 5.63	5.83 \pm 4.64	6.87 \pm 7.86	21.15 \pm 14.26	10.42 \pm 14.27	5.27 \pm 4.29	5.43 \pm 3.82	12.39 \pm 8.12	4.17 \pm 3.6	17.05 \pm 62.15	27.29 \pm 81.62	8.84 \pm 22.63
(nnUNetV2(3D))																	
ESPNet	22.33 \pm 16.56	8.98 \pm 11.86	9.94 \pm 15.51	5.06 \pm 6.34	16.8 \pm 14.66	20.37 \pm 18.03	15.49 \pm 14.52	25.18 \pm 22.03	41.61 \pm 19.34	73.68 \pm 83.07	17.47 \pm 8.02	32.45 \pm 21.58	18.35 \pm 8.25	5.1 \pm 2.74	12.69 \pm 4.91	9.41 \pm 3.49	20.93 \pm 18.13
ESPNet+KD	3.89 \pm 1.12	14.35 \pm 37.18	4.52 \pm 4.65	2.87 \pm 0.91	19.0 \pm 24.07	12.26 \pm 13.69	10.5 \pm 10.36	11.49 \pm 9.72	32.64 \pm 30.05	20.68 \pm 13.62	17.64 \pm 7.75	10.45 \pm 11.4	18.87 \pm 19.96	20.03 \pm 50.47	22.97 \pm 58.09	18.18 \pm 21.9	15.02 \pm 16.3
DMFNet																	
DMFNet+KD	3.45 \pm 0.84	4.63 \pm 7.24	2.91 \pm 0.64	2.61 \pm 0.48	10.83 \pm 9.36	6.21 \pm 6.91	6.17 \pm 4.37	8.23 \pm 8.84	20.32 \pm 13.11	11.11 \pm 12.13	6.59 \pm 4.02	6.75 \pm 4.41	12.48 \pm 6.14	5.3 \pm 4.87	6.58 \pm 6.61	6.1 \pm 5.6	7.52 \pm 3.59
LCOVNet	15.25 \pm 52.03	3.64 \pm 3.95	2.81 \pm 0.74	2.56 \pm 0.45	9.12 \pm 5.49	6.42 \pm 4.86	5.97 \pm 3.23	9.91 \pm 13.95	20.65 \pm 13.35	9.55 \pm 11.72	6.04 \pm 3.6	5.82 \pm 4.44	10.16 \pm 4.55	6.89 \pm 6.67	17.68 \pm 58.9	30.83 \pm 93.82	10.21 \pm 25.87
LCOVNet+KD	5.52 \pm 6.11	4.32 \pm 7.09	3.19 \pm 0.83	2.81 \pm 0.52	15.97 \pm 32.96	11.86 \pm 26.18	7.09 \pm 8.06	8.4 \pm 10.69	19.4 \pm 11.39	12.51 \pm 13.22	6.82 \pm 3.86	6.06 \pm 4.07	12.07 \pm 6.68	6.24 \pm 8.67	17.09 \pm 55.62	6.5 \pm 5.78	9.11 \pm 13.87

Table 7. Comparison between various efficient segmentation methods in term of $HD_{95}(mm)$

Network	Params (M)	MAC (G)	Inference Time (s)
nnUNetV2(3D)	31.18	580.77	0.47
DMFNet	3.87	21.5	0.28
ESPNet	4.45	458.78	0.29
LCOVNet	0.82	100.21	0.21

Table 8. Complexity comparison between various networks. Params and MACs mean the model parameters and multiply-accumulate operations. The MACs and Inference Time are tested on an NVIDIA GTX1080TI GPU with the input size of $64 \times 160 \times 160$.

lowing joint objective function [45, 51, 53],

$$\mathcal{L}_{total} = \mathcal{L}_{pCE} + \lambda_1 \mathcal{L}_{CRF} + \lambda_2 \mathcal{L}_{other} \quad (1)$$

where \mathcal{L}_{other} means other loss functions presented in these works. λ_1 and λ_2 denote the weight factor of these loss functions. These methods have achieved encouraging results in natural image segmentation [42, 43] and salience object detection [53, 51], etc. But for abdominal multi-organ segmentation, learning from scribbles is also a very challenging task. Different from the above, we propose a new regularization term to train deep networks for weakly supervised abdominal multi-organ segmentation.

4.4.2 Entropy minimization

Recently, entropy minimization has been widely used in semi-supervised learning to utilize the unlabeled data [15, 17, 46]. It encourages the model to produce high confidence prediction by minimizing the following object function:

$$\mathcal{L}_{ent} = \sum_c \sum_i -p_c^i \cdot \log p_c^i \quad (2)$$

where p_c^i means the probability value of the pixel i belonging to the c class. In this work, we further use entropy minimization to regularize the deep network for learning from scribble annotations. Our intuition is that the entropy minimization term is more like the pixel-wise contrastive learning to further encourage the model to learn from unlabeled pixels by min-max the intra/inter-class discrepancy. As the softmax prediction has maximized the difference of inter-class and the entropy minimization term enforces the intra-class prediction to be more confident.

4.4.3 Intra-class intensity variance minimization

Although the entropy minimization loss has regularized the deep network at the output level, it does not consider the

image-level information. We hypothesize that the intensity information could bring more useful information and further boost model performance. Here, we attempt to reformat an unsupervised regularization term to consider both prediction and intensity simultaneously. Inspired by the clustering learning [22] and active contour model [3], we propose to regularize the deep network by minimizing the intra-class intensity variance, where the mathematical formulation is defined as:

$$\mathcal{L}_{ivm} = \iint (p_c^i \cdot I^i - u_c)^2 didc \quad (3)$$

where

$$u_c = \frac{\int (I^i \cdot p_c^i) di}{\int p_c^i di} \quad (4)$$

where I^i denotes the intensity value of the input image at pixel i . c is the class number. Based on the above descriptions, the \mathcal{L}_{ivm} can be converted to the intra-class intensity standard deviation minimization term (std).

4.4.4 The overall objective function

In this work, we employ a joint objective function to train model from the scribble annotations, which consists of three terms: partially cross-entropy loss, entropy minimization loss and intensity variance minimization loss and takes the following combination:

$$\mathcal{L}_{total} = \mathcal{L}_{pCE} + \lambda_{ent} \mathcal{L}_{ent} + \lambda_{ivm} \mathcal{L}_{ivm} \quad (5)$$

where λ_{ent} and λ_{ivm} represent the importance of \mathcal{L}_{ent} and \mathcal{L}_{ivm} respectively and both are set to 0.1 in this work.

4.4.5 Experiments and results

Experiments settings: To evaluate the proposed method, we further provide a scribble annotation for the WORD dataset. We generate scribbles for all training volumes in the axial view. Note that the scribble annotations are very sparse in both intra-/inter-slices, which means that not all slices have the scribbles but each organ is annotated at least once in a volume. Due to the scribble annotations based abdominal multi-organ segmentation is not a hot research topic, there is no existing work or openly available codebase. We first build a benchmark for this task and then compare a widely-used method, CRFLoss [43] on the WORD dataset. We use the ResUNet (2D) [10] as our backbone and employ

Method	Liver	Spleen	Kidney(L)	Kidney(R)	Stomach	Gallbladder	Esophagus	Pancreas	Duodenum	Colon	Intestine	Adrenal	Rectum	Bladder	Head of Femur(L)	Head of Femur(R)	Mean
pCE	93.86±0.88	89.43±4.27	87.68±6.48	90.02±4.11	87.09±4.24	62.13±18.78	34.99±10.7	72.27±7.26	52.37±11.07	72.65±10.04	75.37±5.28	36.26±10.2	70.77±10.61	82.77±13.92	73.12±8.65	72.19±8.18	72.06±19.78
pCE+CRF Loss	73.28±3.51	81.71±8.16	92.46±4.17	92.84±4.17	86.64±4.7	63.51±20.52	55.53±12.77	75.27±7.24	56.50±12.57	69.71±5.68	46.09±10.27	28.66±11.83	87.77±16.42	86.5±4.33	87.73±4.14	71.91±20.53	
pCE+EM	92.62±1.67	87.25±5.98	88.68±3.36	89.49±3.78	87.38±3.61	65.21±18.94	41.24±13.38	72.66±7.4	57.74±13.05	76.03±9.99	76.56±5.17	31.44±10.04	70.47±9.86	83.79±16.43	82.39±7.58	82.6±6.74	73.90±19.57
pCE+IVM	88.46±2.48	88.67±6.69	92.02±2.89	90.59±2.55	86.98±4.44	65.09±16.67	54.22±13.09	74.3±7.15	55.06±12.16	74.21±9.84	75.07±4.31	39.86±11.03	71.2±8.08	78.76±13.58	82.41±5.24	82.92±5.34	74.99±17.02
pCE+EM+IVM	90.22±1.92	91.42±3.4	92.13±2.47	92.07±2.78	86.17±2.89	70.64±18.19	62.53±13.1	76.2±6.66	58.47±13.15	78.66±9.38	80.44±3.67	43.46±10.79	69.62±9.55	68.52±11.17	83.85±3.7	84.53±5.31	76.81±16.01
CE+Dice+Mask	96.55±0.89	95.26±2.84	95.63±1.2	95.84±1.16	91.58±2.86	82.83±11.8	77.17±14.68	83.56±5.6	66.67±15.36	83.57±8.69	86.76±3.56	70.9±10.12	82.16±6.73	91.0±13.5	93.39±5.11	93.88±4.30	86.67±4.81

Table 9. Comparison between various weakly-supervised segmentation methods in the term of $DSC(\%)$, all methods based on the same backbone the ResUNet (2D) and same experiment settings.

the nnUNet [21] pipeline to train and test all methods. All implementations and scribble annotations will be released.

Results: The quantitative comparisons between our proposed method and the others are presented in Tab. 9 and Tab. 10. The first interesting observation is that the widely-used CRF Loss [43] achieves a worst performance than all other methods. The reason may be the CRF Loss [43] is specifically designed for natural image segmentation tasks and is not suitable to handle the CT images with low contrast and non-enhancement. Then, we found that the network is capable of leveraging the scribble annotation more efficiently by encouraging to produce more confident predictions. Moreover, compared with the entropy minimization term, our proposed intra-class intensity variance minimization achieves better results, the mean DSC of 73.90% *vs* 74.99%. In addition, by combining the entropy minimization and intra-class intensity variance minimization, the model achieves the best performance than the others and improves the mean DSC from 72.06% to 76.81%. These results demonstrate that also most weakly supervised methods achieve better results than those using partially cross-entropy loss, except for the CRF Loss. It is noteworthy to mention that scribble annotations save more than 96% of label costs than dense annotations. Finally, we find large size organs weakly supervised segmentation results are very close to fully supervised, especially in the liver, spleen, kidney, stomach, head of the femur. However, the small size organs still can not be segmented well, it also points out the research direction going. It also shows that with further research, weakly-supervised learning may further reduce the label costs in the future.

5. Discussion and Conclusion

In this work, we collect and build a large-scale whole abdominal CT multi-organ segmentation dataset containing 150 CT volumes and 16 organs annotation. Although, many abdominal organ segmentation datasets and benchmarks have been established, like AbdomenCT-1K [32], BTCV [23], TCIA [39], LiTS [1], CT-ORG [38], Kits [19], etc, our WORD cover the whole abdominal region and also

Table 10. Comparison between various weakly-supervised segmentation methods in the term of HD_{95} , all methods based on the same backbone the ResUNet (2D) and same experiment settings.

annotate more organs. Then we annotate 20 scans from the open available [1] for clinical applicable and generalizable evaluation. Here, we investigate several hot topics based on the WORD and point out some unsolved problems:

Clinical Applicable Investigation: We investigate several SOTA methods on the WORD dataset and find that all methods can achieve encouraging results. Then, we comprehensively study the clinical acceptance of the deep network. Fig. 3 shows three junior clinical oncologists revise the results. For large scale organs, such as the liver, spleen, kidney, stomach, bladder, head of the femur, the deep network can perform very close to junior clinical oncologists, which means the model prediction can be clinically acceptable after minor revision. However, there are huge performance gaps between junior clinical oncologists and the deep network in small-sized organs, such as the gallbladder, duodenum, adrenal, and rectum. It is tough to apply the model predictions to the clinical application directly, and it requires major revision and careful checks. So, we think the abdominal multi-organ segmentation task is not a well solved problem. But based on the WORD dataset, researchers can focus on handling these challenging organs segmentation to improve performance in clinical practice.

Model Generalization: Recently, domain adaptation and generalization have been scorching topics in the natural/medical image segmentation fields [12, 46]. But for the abdominal multi-organ segmentation task, there are very few studies [11] focused on investigating the generalization problem. This is mainly due to lacking open available multi-sources and large-scale datasets/benchmarks. In this work, we investigate the domain gaps between our build WORD dataset and open-source datasets BTCV [23] and TCIA [39] and find that there are significant domain gaps across different source datasets. Furthermore, we annotated 20 volumes from LiTS [1] as an external evaluation set to validate networks' generalizability and found that the domain gap between LiTS and WORD is not significant. It is desirable to train models with good generalization and high performance to boost deep learning-based clinical applications. So, we build a benchmark for robust and generaliza-

able abdominal multi-organ segmentation research.

Annotation-Efficient Segmentation: Developing an encouraging performance segmentation model always requires many high-quality annotations, but labelling the abdominal multi-organ is very expensive and time-consuming, each volume around takes 1.2-2.6 hours. To reduce the label costs, annotation-efficient learning has attracted many researchers' attention, such as semi-supervised learning [28, 30, 27] and weakly supervised learning [45]. In this work, we propose to learn from the scribble annotation by minimizing the entropy minimization and intra-class intensity variance minimization. Although our proposed method improves the baseline by a large margin, there is also a considerable performance gap compared with dense annotations. In this work, we want to do some attempts to inspire more annotation-efficient researches in the future.

In conclusion, we introduced a new carefully annotated whole abdominal organ CT dataset. Meanwhile, we investigate several existing SOTA methods and perform user studies on this dataset, and further point out some unsolved problems and potential directions in both technique and clinical views. In the future, we will still work on extending the WORD dataset to be more extensive and more diverse.

6. Acknowledgment

This work was supported by the National Natural Science Foundation of China [81771921, 61901084], the National Key Research and Development Program [2020YFB1711503] and also by key research and development project of Sichuan province, China [20ZDZF2817]. We would like to thank Mr. Zhiqiang Hu and Guofeng Lv from the SenseTime Research for constructive discussions and suggestions and also thank M.D. J. Xiao and W. Liao and their team members for data collection, annotation, checking and user study. We also would like to thank the Shanghai AI Lab and Shanghai SenseTime Research for their high-performance computation support.

References

- [1] P. Bilic, P. F. Christ, E. Vorontsov, G. Chlebus, H. Chen, Q. Dou, C.-W. Fu, X. Han, P.-A. Heng, J. Hesser, et al. The liver tumor segmentation benchmark (lits). *arXiv preprint arXiv:1901.04056*, 2019. [2](#), [3](#), [4](#), [6](#), [7](#), [8](#), [10](#)
- [2] H. Cao, Y. Wang, J. Chen, D. Jiang, X. Zhang, Q. Tian, and M. Wang. Swin-unet: Unet-like pure transformer for medical image segmentation. *arXiv preprint arXiv:2105.05537*, 2021. [3](#)
- [3] T. F. Chan and L. A. Vese. Active contours without edges. *TIP*, 10(2):266–277, 2001. [9](#)
- [4] C. Chen, X. Liu, M. Ding, J. Zheng, and J. Li. 3d dilated multi-fiber network for real-time brain tumor segmentation in mri. In *International Conference on Medical Image Computing and Computer-Assisted Intervention*, pages 184–192. Springer, 2019. [7](#)
- [5] J. Chen, Y. Lu, Q. Yu, X. Luo, E. Adeli, Y. Wang, L. Lu, A. L. Yuille, and Y. Zhou. Transunet: Transformers make strong encoders for medical image segmentation. *arXiv preprint arXiv:2102.04306*, 2021. [3](#)
- [6] L.-C. Chen, G. Papandreou, I. Kokkinos, K. Murphy, and A. L. Yuille. Deeplab: Semantic image segmentation with deep convolutional nets, atrous convolution, and fully connected crfs. *IEEE transactions on pattern analysis and machine intelligence*, 40(4):834–848, 2017. [7](#)
- [7] L.-C. Chen, Y. Zhu, G. Papandreou, F. Schroff, and H. Adam. Encoder-decoder with atrous separable convolution for semantic image segmentation. In *ECCV*, pages 801–818, 2018. [2](#), [6](#)
- [8] X. Chen, S. Sun, N. Bai, K. Han, Q. Liu, S. Yao, H. Tang, C. Zhang, Z. Lu, Q. Huang, et al. A deep learning-based auto-segmentation system for organs-at-risk on whole-body computed tomography images for radiation therapy. *Radiotherapy and Oncology*, 160:175–184, 2021. [1](#), [2](#), [6](#)
- [9] Y. Chen, Y. Kalantidis, J. Li, S. Yan, and J. Feng. Multi-fiber networks for video recognition. In *Proceedings of the european conference on computer vision (ECCV)*, pages 352–367, 2018. [7](#)
- [10] F. I. Diakogiannis, F. Waldner, P. Caccetta, and C. Wu. Resunet-a: A deep learning framework for semantic segmentation of remotely sensed data. *ISPRS Journal of Photogrammetry and Remote Sensing*, 162:94–114, 2020. [2](#), [6](#), [9](#)
- [11] Q. Dou, Q. Liu, P. A. Heng, and B. Glocker. Unpaired multi-modal segmentation via knowledge distillation. *TMI*, 39(7):2415–2425, 2020. [10](#)
- [12] Q. Dou, C. Ouyang, C. Chen, H. Chen, and P.-A. Heng. Unsupervised cross-modality domain adaptation of convnets for biomedical image segmentations with adversarial loss. In *IJCAI*, 2018. [10](#)
- [13] Z. Feng, J. Lai, and X. Xie. Resolution-aware knowledge distillation for efficient inference. *TIP*, 30:6985–6996, 2021. [5](#), [7](#)
- [14] E. Gibson, F. Giganti, Y. Hu, E. Bonmati, S. Bandula, K. Gurusamy, B. Davidson, S. P. Pereira, M. J. Clarkson, and D. C. Barratt. Automatic multi-organ segmentation on abdominal ct with dense v-networks. *TMI*, 37(8):1822–1834, 2018. [2](#), [3](#)
- [15] Y. Grandvalet, Y. Bengio, et al. Semi-supervised learning by entropy minimization. *NeurIPS*, 367:281–296, 2005. [9](#)
- [16] D. Guo, D. Jin, Z. Zhu, T.-Y. Ho, A. P. Harrison, C.-H. Chao, J. Xiao, and L. Lu. Organ at risk segmentation for head and neck cancer using stratified learning and neural architecture search. In *CVPR*, pages 4223–4232, 2020. [2](#)
- [17] W. Hang, W. Feng, S. Liang, L. Yu, Q. Wang, K.-S. Choi, and J. Qin. Local and global structure-aware entropy regularized mean teacher model for 3D left atrium segmentation. In *MICCAI*, pages 562–571. Springer, 2020. [9](#)
- [18] A. Hatamizadeh, Y. Tang, V. Nath, D. Yang, A. Myronenko, B. Landman, H. R. Roth, and D. Xu. Unetr: Transformers for 3d medical image segmentation. In *WACV*, pages 574–584, 2022. [2](#), [6](#)
- [19] N. Heller, S. McSweeney, M. T. Peterson, S. Peterson, J. Rickman, B. Stai, R. Tejpaul, M. Oestreich, P. Blake,

J. Rosenberg, et al. An international challenge to use artificial intelligence to define the state-of-the-art in kidney and kidney tumor segmentation in ct imaging., 2020. 10

[20] G. Hinton, O. Vinyals, J. Dean, et al. Distilling the knowledge in a neural network. *arXiv preprint arXiv:1503.02531*, 2(7), 2015. 7

[21] F. Isensee, P. F. Jaeger, S. A. Kohl, J. Petersen, and K. H. Maier-Hein. nnu-net: a self-configuring method for deep learning-based biomedical image segmentation. *Nature methods*, 18(2):203–211, 2021. 2, 5, 6, 7, 10

[22] A. K. Jain and R. C. Dubes. *Algorithms for clustering data*. Prentice-Hall, Inc., 1988. 9

[23] B. Landman, Z. Xu, J. Iglesias, M. Styner, T. Langerak, and A. Klein. Multi-atlas labeling beyond the cranial vault-workshop and challenge. 2017. 2, 3, 6, 7, 8, 10

[24] X. Li, L. Yu, H. Chen, C.-W. Fu, L. Xing, and P.-A. Heng. Transformation-consistent self-ensembling model for semisupervised medical image segmentation. *TNNLS*, 32(2):523–534, 2020. 8

[25] X. Liang, N. Li, Z. Zhang, J. Xiong, S. Zhou, and Y. Xie. Incorporating the hybrid deformable model for improving the performance of abdominal ct segmentation via multi-scale feature fusion network. *MedIA*, 73:102156, 2021. 3

[26] D. Lin, J. Dai, J. Jia, K. He, and J. Sun. Scribble-sup: Scribble-supervised convolutional networks for semantic segmentation. In *CVPR*, pages 3159–3167, 2016. 8

[27] X. Luo. SSL4MIS. <https://github.com/HilLab-git/SSL4MIS>, 2020. 11

[28] X. Luo, J. Chen, T. Song, and G. Wang. Semi-supervised medical image segmentation through dual-task consistency. *AAAI*, 35(10):8801–8809, 2021. 5, 8, 11

[29] X. Luo, M. Hu, T. Song, G. Wang, and S. Zhang. Semi-supervised medical image segmentation via cross teaching between cnn and transformer. In *Medical Imaging with Deep Learning*, 2022. 5

[30] X. Luo, W. Liao, J. Chen, T. Song, Y. Chen, S. Zhang, N. Chen, G. Wang, and S. Zhang. Efficient semi-supervised gross target volume of nasopharyngeal carcinoma segmentation via uncertainty rectified pyramid consistency. In *MICCAI*, pages 318–329, 2021. 8, 11

[31] X. Luo, G. Wang, T. Song, J. Zhang, M. Aertsen, J. Deprest, S. Ourselin, T. Vercauteren, and S. Zhang. Mideepseg: Minimally interactive segmentation of unseen objects from medical images using deep learning. *MedIA*, 72:102102, 2021. 6

[32] J. Ma, Y. Zhang, S. Gu, C. Zhu, C. Ge, Y. Zhang, X. An, C. Wang, Q. Wang, X. Liu, et al. Abdomenct-1k: Is abdominal organ segmentation a solved problem. *TPAMI*, 2021. 2, 3, 4, 10

[33] A. Mishra and D. Marr. Apprentice: Using knowledge distillation techniques to improve low-precision network accuracy. *arXiv preprint arXiv:1711.05852*, 2017. 5

[34] N. Rueckert, S. Ourselin, and S. Mehta. 3d-espnet with pyramidal refinement for volumetric brain tumor image segmentation. In *International MICCAI Brainlesion Workshop*, pages 245–253. Springer, 2018. 7

[35] O. Oktay, J. Schlemper, L. L. Folgoc, M. Lee, M. Heinrich, K. Misawa, K. Mori, S. McDonagh, N. Y. Hammerla, B. Kainz, et al. Attention u-net: Learning where to look for the pancreas. *arXiv preprint arXiv:1804.03999*, 2018. 2, 6

[36] A. Paszke, S. Gross, F. Massa, A. Lerer, J. Bradbury, G. Chanan, T. Killeen, Z. Lin, N. Gimelshein, L. Antiga, et al. Pytorch: An imperative style, high-performance deep learning library. In *NeurIPS*, pages 8026–8037, 2019. 5

[37] D. Qin, J.-J. Bu, Z. Liu, X. Shen, S. Zhou, J.-J. Gu, Z.-H. Wang, L. Wu, and H.-F. Dai. Efficient medical image segmentation based on knowledge distillation. *IEEE Transactions on Medical Imaging*, 40(12):3820–3831, 2021. 7

[38] B. Rister, D. Yi, K. Shivakumar, T. Nobashi, and D. L. Rubin. Ct-org, a new dataset for multiple organ segmentation in computed tomography. *Scientific Data*, 7(1):1–9, 2020. 2, 3, 4, 10

[39] H. R. Roth, L. Lu, A. Farag, H.-C. Shin, J. Liu, E. B. Turkbey, and R. M. Summers. Deeporgan: Multi-level deep convolutional networks for automated pancreas segmentation. In *MICCAI*, pages 556–564. Springer, 2015. 2, 3, 6, 7, 8, 10

[40] J. Schlemper, O. Oktay, M. Schaap, M. Heinrich, B. Kainz, B. Glocker, and D. Rueckert. Attention gated networks: Learning to leverage salient regions in medical images. *MedIA*, 53:197–207, 2019. 3

[41] H. Tang, X. Chen, Y. Liu, Z. Lu, J. You, M. Yang, S. Yao, G. Zhao, Y. Xu, T. Chen, et al. Clinically applicable deep learning framework for organs at risk delineation in ct images. *Nature Machine Intelligence*, 1(10):480–491, 2019. 1

[42] M. Tang, A. Djelouah, F. Perazzi, Y. Boykov, and C. Schroers. Normalized cut loss for weakly-supervised cnn segmentation. In *CVPR*, pages 1818–1827, 2018. 8, 9

[43] M. Tang, F. Perazzi, A. Djelouah, I. Ben Ayed, C. Schroers, and Y. Boykov. On regularized losses for weakly-supervised cnn segmentation. In *ECCV*, pages 507–522, 2018. 8, 9, 10

[44] Y. Tang, R. Gao, H. H. Lee, S. Han, Y. Chen, D. Gao, V. Nath, C. Bermudez, M. R. Savona, R. G. Abramson, et al. High-resolution 3d abdominal segmentation with random patch network fusion. *MedIA*, 69:101894, 2021. 3, 5, 7

[45] G. Valvano, A. Leo, and S. A. Tsaftaris. Learning to segment from scribbles using multi-scale adversarial attention gates. *TMI*, 2021. 8, 9, 11

[46] T.-H. Vu, H. Jain, M. Bucher, M. Cord, and P. Pérez. Advent: Adversarial entropy minimization for domain adaptation in semantic segmentation. In *CVPR*, pages 2517–2526, 2019. 9, 10

[47] G. Wang, M. A. Zuluaga, W. Li, R. Pratt, P. A. Patel, M. Aertsen, T. Doel, A. L. David, J. Deprest, S. Ourselin, et al. Deepigeos: a deep interactive geodesic framework for medical image segmentation. *TPAMI*, 41(7):1559–1572, 2018. 6

[48] Y. Wang, Y. Zhou, W. Shen, S. Park, E. K. Fishman, and A. L. Yuille. Abdominal multi-organ segmentation with organ-attention networks and statistical fusion. *MedIA*, 55:88–102, 2019. 2, 3

[49] Y. Xia, D. Yang, Z. Yu, F. Liu, J. Cai, L. Yu, Z. Zhu, D. Xu, A. Yuille, and H. Roth. Uncertainty-aware multi-view

co-training for semi-supervised medical image segmentation and domain adaptation. *MedIA*, 65:101766, 2020. 8

[50] Y. Xie, J. Zhang, C. Shen, and Y. Xia. Cotr: Efficiently bridging cnn and transformer for 3d medical image segmentation. In *MICCAI*, pages 171–180. Springer, 2021. 2, 6

[51] S. Yu, B. Zhang, J. Xiao, and E. G. Lim. Structure-consistent weakly supervised salient object detection with local saliency coherence. In *AAAI*, 2021. 9

[52] P. A. Yushkevich, J. Piven, H. C. Hazlett, R. G. Smith, S. Ho, J. C. Gee, and G. Gerig. User-guided 3d active contour segmentation of anatomical structures: significantly improved efficiency and reliability. *Neuroimage*, 31(3):1116–1128, 2006. 4

[53] J. Zhang, X. Yu, A. Li, P. Song, B. Liu, and Y. Dai. Weakly-supervised salient object detection via scribble annotations. In *CVPR*, pages 12546–12555, 2020. 9

[54] X. Zhang, X. Zhou, M. Lin, and J. Sun. Shufflenet: An extremely efficient convolutional neural network for mobile devices. In *Proceedings of the IEEE conference on computer vision and pattern recognition*, pages 6848–6856, 2018. 7

[55] Q. Zhao, H. Wang, and G. Wang. Lcov-net: A lightweight neural network for covid-19 pneumonia lesion segmentation from 3d ct images. In *2021 IEEE 18th International Symposium on Biomedical Imaging (ISBI)*, pages 42–45. IEEE, 2021. 7

[56] Y. Zhou, Z. Li, S. Bai, C. Wang, X. Chen, M. Han, E. Fishman, and A. L. Yuille. Prior-aware neural network for partially-supervised multi-organ segmentation. In *ICCV*, pages 10672–10681, 2019. 3, 7

[57] Y. Zhou, Y. Wang, P. Tang, S. Bai, W. Shen, E. Fishman, and A. Yuille. Semi-supervised 3d abdominal multi-organ segmentation via deep multi-planar co-training. In *WACV*, pages 121–140. IEEE, 2019. 3, 5

[58] Z. Zhou, M. M. R. Siddiquee, N. Tajbakhsh, and J. Liang. Unet++: Redesigning skip connections to exploit multiscale features in image segmentation. *TMI*, 39(6):1856–1867, 2019. 2, 6